

**FLEXURAL STRENGTH AND HINGE BEHAVIOR OF
INTERNALLY POST-TENSIONED MEMBERS WITH MIXED
BONDED AND UNBONDED TENDONS**

By

NATASSIA R. BRENKUS, H.R. HAMILTON, AND
WILL A. POTTER



Authorized reprint from: December 2017 issue of the PTI Journal

Copyrighted © 2017, Post-Tensioning Institute
All rights reserved.

FLEXURAL STRENGTH AND HINGE BEHAVIOR OF INTERNALLY POST-TENSIONED MEMBERS WITH MIXED BONDED AND UNBONDED TENDONS

BY NATASSIA R. BRENKUS, H.R. HAMILTON, AND WILL A. POTTER

The use of flexible filler materials in internal post-tensioning tendons—an alternative to the more typical cementitious grout that is currently common in U.S. post-tensioned bridge construction—has implications to the member’s flexural strength behavior and design. When using flexible fillers, a unique design situation is encountered in certain types of bridge construction: I-girder members containing both internal tendons of unbonded post-tensioned steel and bonded pretensioned steel. AASHTO-LRFD (2016) provides a simplified approach for components with bonded and unbonded tendons, but this design situation has not yet been commonly used in bridge practice and has not been investigated in research programs. This paper describes the experimental testing and observations of two beam specimens with both bonded pretensioned steel and unbonded post-tensioned steel. Comparison is made to a fully bonded member, and to the anticipated design strength using the current provisions of AASHTO-LRFD (2016).

KEYWORDS

bridge; flexible filler; mixed tendons; plastic hinge; post-tensioning; prestressing; unbonded.

INTRODUCTION

The use of flexible fillers in post-tensioned bridge construction is new to the United States and is being investigated by several state departments of transportation for the materials’ potential as a possible component of the corrosion protection system, with aims to improve structural system durability and to simplify tendon inspection, maintenance, or replacement.

The use of flexible filler materials, in lieu of grout, results in a structural system reinforced with unbonded tendons. When comparing the flexural behavior of beams with only bonded tendons to those with only unbonded tendons, significant behavioral differences occur only when the beam is loaded beyond cracking. Once cracking occurs in bonded tendon members, the stress-strain compatibility due to the concrete-steel bond ensures that the accumulated tensile strain occurring at a crack is concentrated, resulting in large localized stress increases in the tendon over the crack length. Conversely, in members with unbonded tendons, tensile strain associated with cracking is distributed over the full length of the tendon (or between deviation points); although cracks may be relatively wide in unbonded members (compared with those seen in bonded members), the resulting increase in overall tendon stress is comparatively small. This difference results in higher flexural strengths at smaller deflections for bonded tendon members versus larger crack opening and lower strength for unbonded tendon members (Gerber and Burns 1971). To obtain the same flexural strength in the same size section of an unbonded tendon system, additional unbonded tendons or mild steel (or both) are required.

Determining the steel stress in bonded post-tensioning tendons at flexural strength can be accomplished through first principles. The fundamental assumption that the prestressing steel is perfectly bonded to the concrete is a prerequisite for this approach and allows the flexural strength to be computed at a chosen section. Unbonded tendons, on the other hand, must be evaluated at the member—rather than the section—level. Because unbonded tendons transfer stress only at anchorages and other points of contact, consideration must be made of the

PTI JOURNAL, V. 13, No. 2, December 2017. Received and reviewed under Institute journal publication policies. Copyright ©2017, Post-Tensioning Institute. All rights reserved, including the making of copies unless permission is obtained from the Post-Tensioning Institute. Pertinent discussion will be published in the next issue of *PTI JOURNAL* if received within 3 months of the publication.

tendon profile, load pattern, friction, and member geometry to evaluate tendon stress.

MacGregor et al. (1989) conducted flexural testing of quarter-scale, precast segmental concrete box-girder continuous span specimens to assess flexural strength in specimens with external tendons to evaluate unbonded tendon stress (MacGregor et al. 1989; Roberts-Wollman et al. 2005). Based on this work, an equation was developed for estimating tendon stresses in members with only unbonded tendons; this equation was later adopted into the AASHTO-LRFD Bridge Design Specifications (AASHTO 2016; Roberts-Wollman et al. 2005). Comparing the flexural strength of segmental members with external tendons filled with wax versus external tendons filled with grout, Hoang and Pasquignon (1985) found slightly lower strength exhibited by the unbonded member.

Although much research has been done on members with either bonded or unbonded post-tensioning tendons, members with both bonded and unbonded tendons have received little consideration in the literature or in experimental testing beyond providing a counterpoint to members with only one type of tendon. Gauvreau (1992) proposed a model for the rational calculation of tendon stress at flexural strength for members with bonded reinforcement, unbonded tendons, or both, based on a truss model with explicit consideration of the angle of inclination of the internal concrete compression chords. The approach relates the global structural deformations (used to calculate the elongation of the unbonded prestressing steel) to the strain state corresponding to the internal forces in the truss at any given section. The proposed method was compared with experimental load tests of eight simply supported concrete girders. To the authors' knowledge, Gauvreau's (1992) proposed rational approach has not been acknowledged in subsequent research or incorporated into design standards to date.

Seismic tests by Megally et al. (2002) were conducted on precast segmental bridge superstructures with different post-tensioning systems (internal, external, and mixed). They suggested a combination of internal bonded tendons and external tendons (mixed tendons) should not be used, as the combination neither improves the strength nor the ductility when compared to members with only bonded internal tendons.

AASHTO-LRFD

Structural members containing both bonded and unbonded tendons have not yet been rationally approached in design standards, nor has a model for

determining their nominal flexural strength been adopted. Design of components with both bonded and unbonded tendons is treated only briefly in the current AASHTO-LRFD design specifications (AASHTO 2016) in Article 5.7.3.1.3, without expressly described justification. The provision states that either a "simplified" or a "detailed" approach be undertaken by the designer to assess the unbonded and bonded steel stress. The guidance given for the detailed analysis is that the designer perform an analysis that "shall take into account the strain compatibility between the section and the bonded prestressing steel. The stress in the unbonded prestressing steel shall take into account the global displacement compatibility between bonded sections of tendons located within the span. Bonded sections of unbonded tendons may be anchorage points and any bonded section, such as deviators... [sic]" and "the nominal flexural strength should be computed directly from the stresses resulting from this analysis". Else, a second provision introduces a "conservative" simplified approach with the following method: 1) the stress in the unbonded tendon at flexural strength is estimated as the effective prestress after losses f_{pe} ; 2) the stress in the bonded prestressing is then determined by Eq. (5.7.3.1.1-1) through (5.7.3.1.1-4) (given as follows), with the term $A_{ps}f_{pu}$ in Eq. (5.7.3.1.1-3) and (5.7.3.1.1-4) replaced with $A_{psb}f_{pu} + A_{psu}f_{pe}$; and 3) a weighted average of the bonded and unbonded steel stress is considered to act over the total area of prestressing steel. Equations (5.7.3.1.1-1) through (5.7.3.1.1-4) are given as Eq. (1) through (4), respectively, as follows

$$f_{ps} = f_{pu} \left(1 - k \frac{c}{d_p} \right) \quad (1)$$

In which

$$k = 2 \left(1.04 - \frac{f_{py}}{f_{pu}} \right) \quad (2)$$

For T-section behavior

$$c = \frac{A_{ps}f_{pu} + A_s f_s - A'_s f'_s - 0.85 f'_c (b - b_w) h_f}{0.85 f_c \beta_1 b + k A_{ps} \frac{f_{pu}}{d_p}} \quad (3)$$

For rectangular section behavior

$$c = \frac{A_{ps}f_{pu} + A_s f_s - A'_s f'_s}{0.85f_c\beta_1 b + kA_{ps} \frac{f_{pu}}{d_p}} \quad (4)$$

EXPERIMENTAL METHOD

To assess the influence of alternative, non-cementitious filler materials on the overall structural behavior (serviceability and strength), laboratory testing was conducted on three full-size beam specimens with both pretensioned and post-tensioned strand. Two beam specimens with an unbonded tendon (filled with flexible filler material) were compared to a control specimen containing a bonded (grouted) tendon.

Test Specimens

Three 40 ft (12 m) long, simple-span precast concrete I-girders with an 8 x 34 in. (200 x 860 mm) deck were constructed, each with three bonded 0.6 in. (15 mm) diameter pretensioned strands and a parabolic, internal post-tensioned tendon composed of twelve 0.6 in. (15 mm) diameter prestressing strands; the strand quantities were selected based on the laboratory testing capabilities. The chosen cross section was a modified AASHTO shape, selected because the precaster’s formwork for this shape accommodated the tendon; by using the side forms of a Type IV with the bottom form of a Type V, the resulting 10 in. wide web fit the internal tendon with the minimum specified concrete cover (2 in. [51 mm], per Florida Department of Transportation guidelines). End blocks were constructed in a second placement to house the anchorages. The tendon duct was a 3 in. (76 mm) diameter, DR 17 smooth high-density polyethylene (HDPE) for the flexible filler specimens and 3 in. (76 mm) diameter corrugated plastic duct for the grouted specimen; the duct materials were selected to reflect the types used in current practice (corrugated with grout) and the new practice (smooth HDPE with flexible filler, specified so as to withstand the heat during injection). The specified compressive strength for both the girder and deck concrete was 8.5 ksi (59 MPa); the test-day material strengths are given in Table 1. All prestressing strand was seven-wire, Grade 270, low-relaxation steel. The test specimen cross section is shown in Fig. 1. The naming convention and key parameters are described in Table 2.

Post-Tensioning and Filler Injection

The deck was placed at the lab prior to post-tensioning. Each strand of the post-tensioning tendon was stressed incrementally using a monostrand jack from one end to a specified prestress of $0.8f_{pu}$. A hollow-core load cell was placed in line with the tendon and used to directly measure the post-tensioning force (Fig. 2). Following post-

Table 1—Test-day concrete compressive strength

Specimen	Deck, ksi	Girder, ksi
IGS	10.3	13.2
IWS	10.3	13.2
IWC	13.7	13.2

(Note: 1 ksi = 6.9 MPa)

Table 2—Key parameters

Specimen	Tendon type	Filler material	Loading configuration
IGS	Internal bonded	Grout	Single point
IWS	Internal unbonded	Flexible Filler	Single point
IWC	Internal unbonded	Flexible Filler	Constant moment

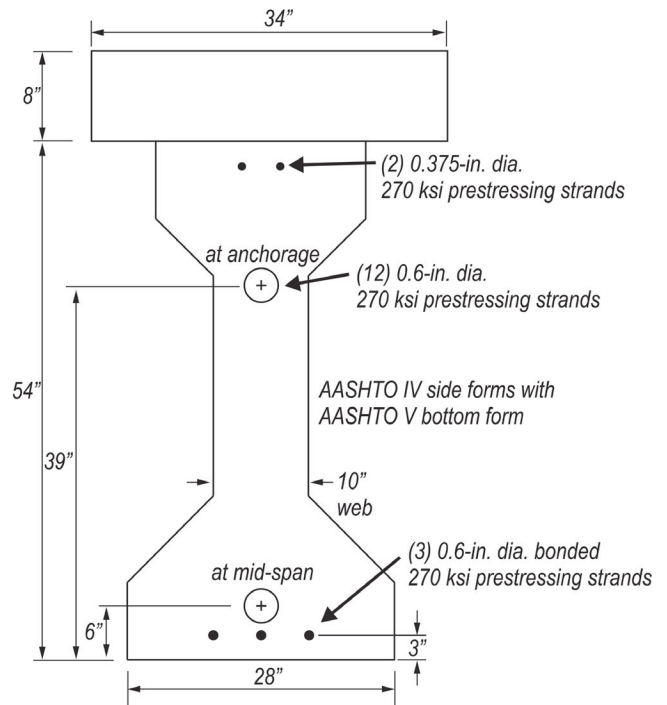


Fig. 1—Internal tendon test specimens. (Note: 1 in. = 25.4 mm; 270 ksi = 1860 MPa.)

tensioning, the tendon was injected with a filler material; two specimens were injected with a microcrystalline, petroleum-derived flexible filler and one specimen was injected with a commercially available cementitious cable grout. Table 3 summarizes the measured tendon force at time of post-tensioning and at time of the load test.

Testing Procedures and Instrumentation

Static ultimate flexure tests were performed on each specimen. Specimens IGS and IWS were tested in a three-

point bending setup and Specimen IWC was tested in four-point bending. The test setups are shown in Fig. 3.



Fig. 2—Load cell (left) in line with anchorage during injection (right).

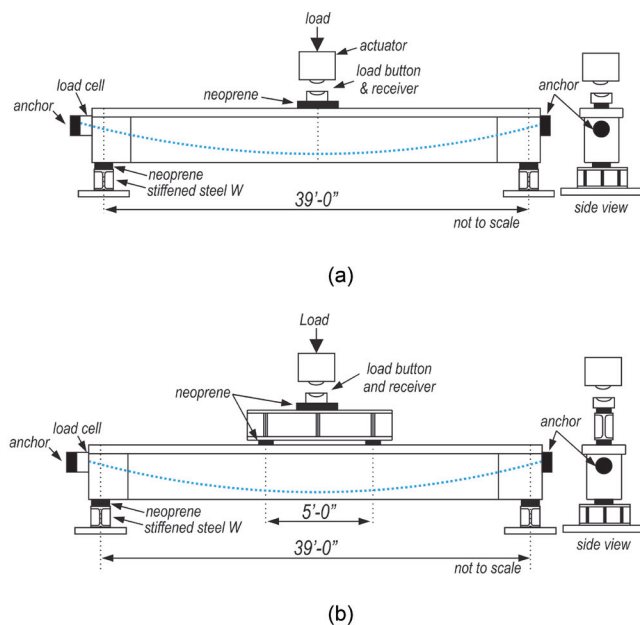


Fig. 3—Flexural test setup: (a) IGS and IWS; and (b) IWC. (Note: 1 in. = 25.4 mm.)

Table 3—Post-tensioning force

Specimen	Initial		At time of load test	
	Average PT tendon force*, kip	Average tendon stress†, ksi	Average PT tendon force*, kip	Average tendon stress†, ksi
IGS	438	$0.62f_{pu}$	424	$0.60f_{pu}$
IWS	426	$0.61f_{pu}$	412	$0.58f_{pu}$
IWC	435	$0.62f_{pu}$	428	$0.61f_{pu}$

*Measured via hollow-core load cell.

† f_{pu} assumed to be 270 ksi.

Note: 1 kip = 454 kg; 1 ksi = 6.9 MPa.

Instrumentation included displacement gauges to measure beam displacement, load cells to measure applied load, and strain gauges to monitor concrete compressive strain in the deck. A key, unique feature of the testing was the direct measurement of the post-tensioning tendon force during the load test (Fig. 2).

In each test, load was applied at 0.2 kip/s (0.9 kN/s). When cracking was first visually observed, the load was held. The beam was then completely unloaded to install additional instrumentation. Load application was then reapplied at 0.4 kip/s (1.8 kN/s) until the approximate cracking load, when the load rate was reduced to 0.2 kip/s (0.9 kN/s) until the termination of the test. The test was terminated when either compressive failure occurred in the deck concrete (bonded specimen IGS) or when the bonded prestressing strands ruptured (mixed tendon specimens IWS and IWC). In all tests, the flexural strength (maximum load) was reached prior to the end of the test.

Service and Cracking Behavior

To highlight the elastic behavior of the internal tendon specimens, Fig. 4 shows the moment-displacement plot from the first load ramp (during which each beam was loaded until visible cracking); the cracking loads are identified as the slope change on the plot. For clarity, beam unloading is not shown. The secondary y-axis shows the ratio of the calculated bottom fiber stress to $\sqrt{f'_c}$ (psi). The extreme bottom fiber stress was calculated with the following assumptions:

- Bonded prestressing strand— f_{se} based on the initial prestress reported in the precaster's stressing records minus an assumed prestress loss of 20% and the area of the prestressing strand, as reported in the material certifications.
- Post-tensioning tendon— f_{se} determined from the hollow-core load cell readings and area of the prestressing strand as reported in the material certifications.

The load level corresponding to the extreme fiber tensile stress for the AASHTO-LRFD Service III limit state ($0.19\sqrt{f'_c}$ ksi [550 psi (3.8 MPa)]) and the cracking limit at ($7.5\sqrt{f'_c}$ psi [690 psi (4.8 MPa)]) are shown for reference, assuming the specified concrete compressive strength (8500 psi [59 MPa]). Each specimen behaved linear-elastically until cracking, and all specimens exhibited approximately the same uncracked stiffness.

The observed cracking loads were determined from the data as the occurrence of a slope change in the plot of load versus midspan displacement. The anticipated cracking loads (applied jack load) were assumed to occur at an

extreme bottom fiber tensile stress of $7.5\sqrt{f'_c}$ (psi), and were determined using transformed composite section properties, test-day material strengths, the effective prestress in the pretensioned bonded steel based on stressing records minus AASHTO-LRFD prestress loss estimates (for bonded steel, per AASHTO 2016), and the load cell readings for the unbonded post-tensioned tendon (Table 4). In all cases, the specimens exhibited first cracking prior to the anticipated cracking loads. Cause of the low cracking load was investigated, but none was identified (for additional discussion, refer to the FDOT report). Cracking stresses of 2.2 to $3.8\sqrt{f'_c}$ psi have been observed by the researchers in past laboratory testing (Brenkus et al. 2016).

Figure 5 shows the final cracking patterns; the first crack location of each specimen is a thick red line. All specimens first developed a flexural crack near the midspan. As loading progressed, cracks in Specimen IGS were noted to be uniformly distributed beneath the load point, typical of bonded prestressed beam behavior. Conversely, both IWS and IWC exhibited behavior more typical of unbonded, prestressed beams: fewer cracks developed overall, and those cracks opened widely as the loading progressed. Specimen IWC developed a wider distribution of cracks compared to IWS due to the different loading configurations.

Strength

The moment versus midspan displacement from the flexural strength tests of all specimens is shown in Fig. 6. The flexural strength of the internal tendon specimens was calculated per AASHTO-LRFD (2016) and is given in Table 5. The strength of bonded member IGS, computed in accordance with AASHTO-LRFD (2016) bonded provisions using test-day material strengths, was 4165 kip-ft (61 MN/m). The observed flexural strength of grouted Specimen IGS, considering self-weight, was 4384 kip-ft (64 MN/m), exceeding the calculated flexural strength by approximately 5%.

For the unbonded specimens IWS and IWC, the AASHTO-LRFD (2016) flexural strength was calculated using Article 5.7.3.1.3b, which provides a simplified approach to approximate the tendon stress for members with both bonded and unbonded components. The calculated nominal flexural strengths M_n , incorporating test-day material properties, were 3830 kip-ft (56 kN/m) for IWS and 4030 kip-ft for IWC. The observed flexural strength of IWS and IWC was approximately 3565 and 3956 kip-ft (52 and 58 MN/m), respectively. Neither IWS nor IWC resisted the calculated

AASHTO-LRFD flexural strength by the simplified approach (AASHTO 2016). As expected, the bonded specimen resisted greater moment by approximately 25% and 10% compared to specimens mixed tendon specimens, respectively.

Specimen IWC underwent much greater displacement at a higher strength compared to IWS, although the two specimens were detailed and constructed in the same manner. The differing behavior can be attributed to the loading scheme—IWS was loaded in a three-point bending setup and IWC was subjected to a four-point scheme—and the consequent development of the plastic region or hinge length. The constant moment region created a longer hinge length than a single concentrated force. The hinge length, which affects the member’s rotational capacity, has apparent implications on the flexural strength and deflection of members with mixed tendons.

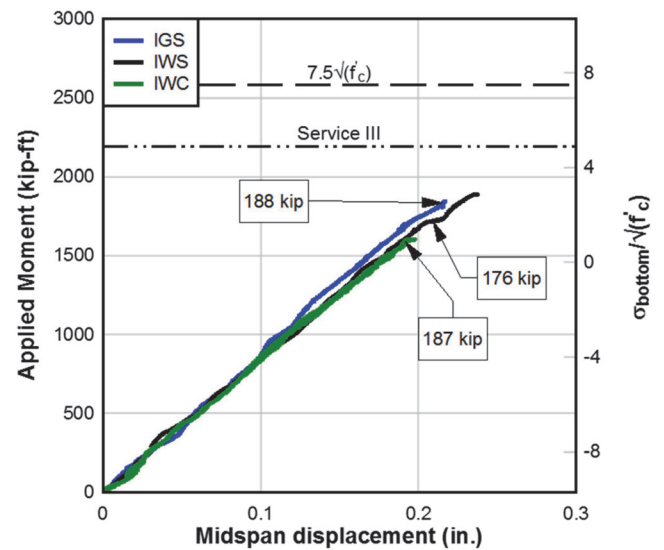


Fig. 4—Elastic behavior. (Note: 1 in. = 25.4 mm; 1 kip = 454 kg.)

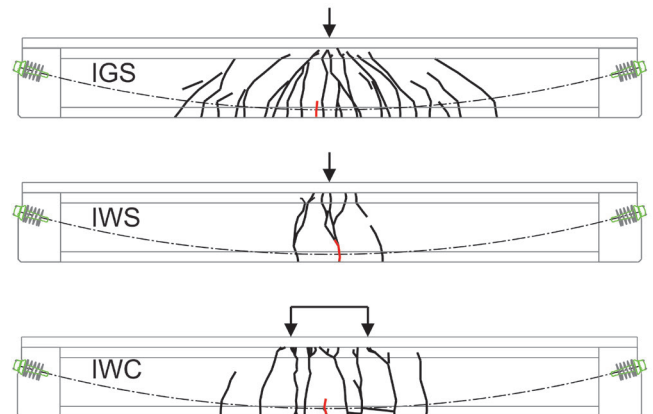


Fig. 5—Final cracking patterns.

DISCUSSION

When loaded to flexural strength, a post-tensioned beam with an unbonded tendon exhibits different behavior than an otherwise equivalent beam with a bonded tendon (Fig. 7). An unbonded beam develops fewer cracks and those cracks are of larger widths than those of a bonded beam. Further, an unbonded beam also has less post-

cracking stiffness and undergoes greater deflection as it approaches maximum load compared to a bonded beam. Specimens IWS and IWC—and the drop-in I-girder construction the specimens mimic—have both unbonded post-tensioned tendons and bonded pretensioned steel. The observed service and strength behavior of members with mixed bonded and unbonded prestressing steel is somewhere between a fully bonded case and an unbonded case: the mixed tendon test specimens IWS and IWC developed fewer cracks (versus a single theoretical crack in unbonded members, or versus many cracks, as in bonded test specimen IGS), and exhibited a lower strength.

Strength of an unbonded system, or the now-considered mixed tendon system, is dependent on the unbonded tendon stress, which is, in turn, dependent on several parameters, including: constitutive material properties, span-depth ratio, tendon profile, bonded-to-unbonded steel area ratio, loading, and length of the plastic hinge. Several of these contributing factors are now discussed.

Influence of material properties—The behavior of members with both unbonded prestressing strand and bonded mild (Grade 60, typically) steel reinforcement—also sometimes referred to as partially prestressed members—provides some insight into components with mixed tendons (both bonded and unbonded prestressing strand), but the use of bonded Grade 270 prestressing steel has several implications:

- Prestressing strand begins to yield (begins plastic hinge formation) at higher tendon stress versus mild steel, allowing greater overall beam displacement prior to steel nonlinearity; and
- The rupture of prestressing strand occurs at a lower strain than the rupture of mild steel. As a result,

members with mixed tendons have a lower rotational capacity compared to that expected of prestressed members with supplementary mild steel.

Figure 8 presents the tested reinforcement schemes and the corresponding conceptual stress state of the reinforcement at the strength limit state. In general, all bonded reinforcement (regardless of the steel grade) experiences a concentrated strain increase at a crack location. In members with unbonded rein-

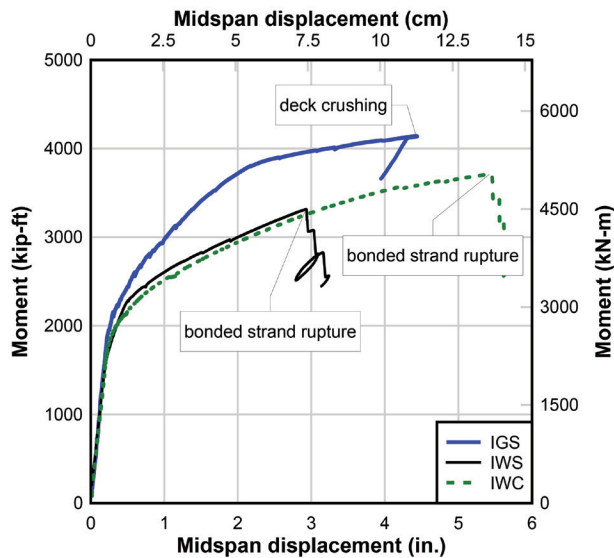


Fig. 6—Flexural strength.

Table 4—Cracking load

Specimen	Crack type	Anticipated cracking load, kip	Measured cracking load, kip
IGS	Flexural	259	188
IWS	Flexural	255	176
IWC	Flexural	298*	187

*Four-point bending.

Note: 1 kip = 454 kg.

Table 5—Flexural strength

Specimen	AASHTO-LRFD article	Calculated		Observed			Cracked length of bottom flange, in.
		M_n , kip-ft	f_{ps} , ksi	M_n , kip-ft	f_{ps} , ksi	Δ , in.	
IGS	Bonded	4165	280	4384	162	4.4	248
IWS	Simplified mixed	3830	259	3565	229	2.9	47
IWC	Simplified mixed	4030	263	3956	274	5.5	95

Note: 1 kip = 454 kg; 1 in. = 25.4 mm; 1 ksi = 6.9 MPa.

forcement, in contrast, the opening of a crack exposes the entire unbonded tendon to the increasing strain, which is distributed along the entire tendon length and results in a theoretically uniform unbonded tendon stress.

In the case of mixed tendons—bonded prestressing steel with unbonded prestressing steel—the general concept of concentrated strain increases at crack locations is the same as with members with mild reinforcement and unbonded prestressing reinforcement. Two differences, however, impact the behavior: the steel grade and the prestrain due to prestressing. For the following discussion, commonly used steel grades in bridge construction will be considered: ASTM A615 Grade 60 for mild steel,

and ASTM A416 seven-wire prestressing strand Grade 270 for prestressing strand.

Prestressing steel yields at a greater strain than mild steel (approximately 0.01 in./in. versus 0.002 in./in.) Despite the prestrain in the bonded prestressing steel, prestressing steel has greater strain available prior to yield, leading to greater load-carrying potential—as well as rotational capacity prior to steel yield—of a specimen reinforced with prestressing steel versus mild steel (steel strain from start of load application until yield is approximately 0.005 in./in. versus 0.002 in./in., respectively).

The difference in rupture strain is of greater significance; a typical set of strain values is considered in this discussion. Mild steel ruptures at strains of approximately 0.14 in./in., while prestressing steel experiences rupture at strains of approximately 0.06 in./in.—approximately half. The implication is that mild steel rupture is unlikely to control the failure behavior. Meanwhile, as observed in the testing, rupture of the prestressing steel is a possible failure mechanism and deserves consideration in members with both bonded and unbonded prestressed components.

Plastic Hinge—Just as is the case in members with only unbonded tendons, the hinge rotation limits the plastic behavior of a member with mixed bonded and unbonded tendons. As with unbonded members, the flexural strength of members with mixed tendons can be described through this rotation capacity, described by the

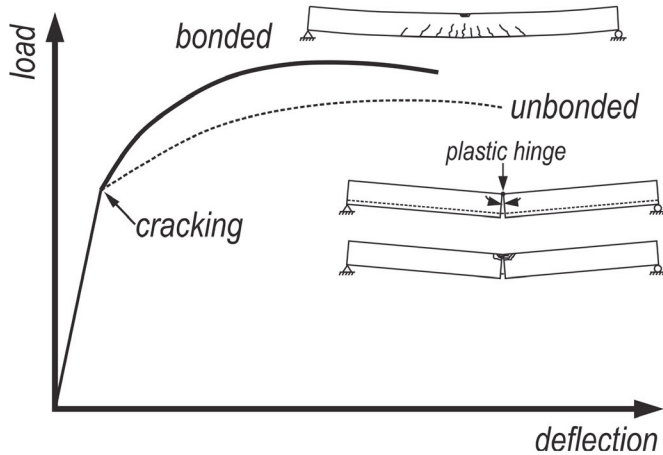


Fig. 7—Theoretical bonded versus unbonded behavior.

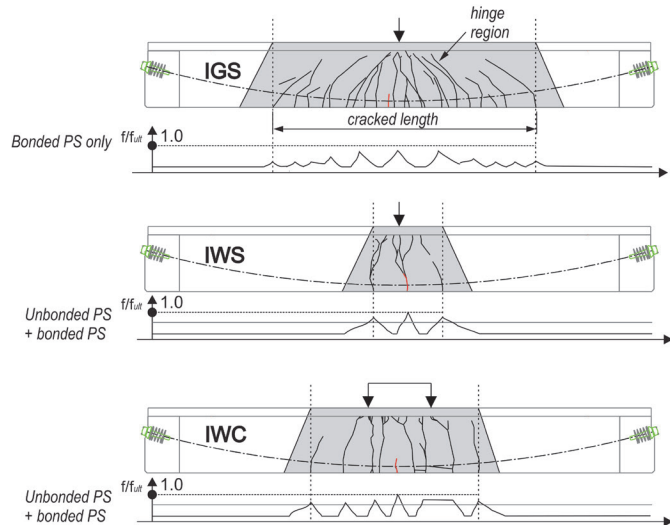
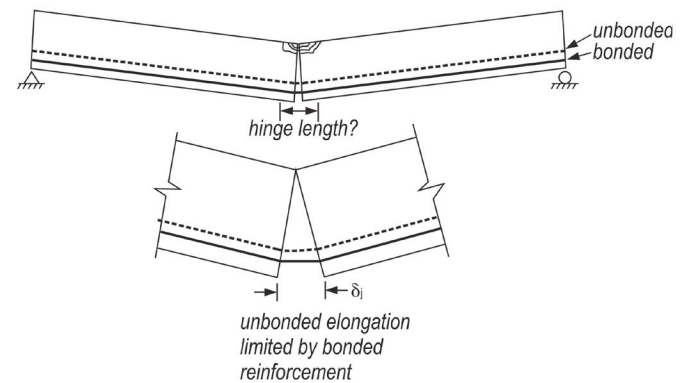


Fig. 8—Tendon stress in different reinforcement conditions.

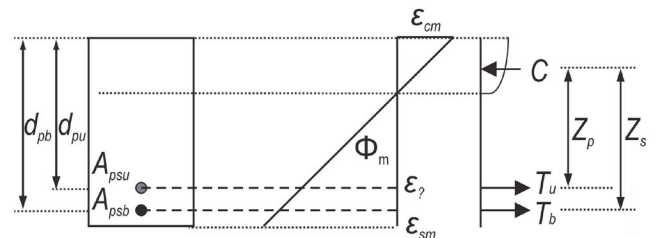


Fig. 9—Hinge development with mixed tendons.

limiting strains of the concrete in compression and the bottom prestressing strand in tension. The limit state is described as the maximum curvature

$$\Phi_m = \frac{\epsilon_{cm} + \epsilon_{sm}}{d_s} \quad (5)$$

where ϵ_{cm} is the maximum concrete compressive strain and ϵ_{sm} is the maximum steel strain; and d_s is the distance from the extreme compression fiber to the bonded pretensioned steel.

Unlike an idealized hinge, which has unlimited rotation ability, the hinge rotation in a reinforced beam is controlled by the limiting strains of the concrete (in compression) and the reinforcement (in tension) (Fig. 9). Concrete compressive strains are limited to the crushing strain, while the tensile strain of the steel reinforcement is limited to rupture strain. In previous investigations by others (Gerber and Burns 1971; Mattock et al. 1971; Ozkul et al. 2008, for example) of unbonded tendons

where mild steel was considered, the limiting tensile strain was great enough that it was unlikely to control the rotational capacity of the hinge.

Tendon elongation at flexural strength and, by association, the tendon stress at the hinge, is a function of both the maximum curvature and the available steel gauge length, which is dependent on the bond condition of the reinforcement (Fig. 10; MacGregor et al. 1989).

The unbonded tendon stress calculations given by AASHTO-LRFD (2016) consider an assumed hinge length equal to twice the distance from compressive force resultant to the bonded reinforcement (or $2Z_s$) as a part of the derivation of the unbonded stress calculation (MacGregor et al. 1989); the hinge failure mechanism is shown in Fig. 9 and 11. The assumed hinge length does not account for distributed loading, nor does it incorporate other factors in the hinge development, such as the presence of bonded reinforcement. In a bonded tendon, the affected region, or gauge length, is assumed to be limited to the joint opening plus twice the development length of the reinforcement. In contrast, unbonded tendon stress increases along the length of the tendon between attachment points or anchors, as in the currently discussed mixed tendon case. The increase in unbonded tendon stress for mixed tendons lightly reinforced with bonded steel is effectively limited by the elongation of the bonded reinforcement over its gauge length (Fig. 10).

A plastic hinge in a reinforced concrete beam is defined as the portion of the member in which the reinforcement has yielded, exhibiting a nonlinear response; at flexural strength, the length of the yielded steel is considered the plastic hinge length. Given the constitutive materials' nonlinearity, geometric irregularities inherent in construction, and high strain localization in the plastic zone, the actual plastic hinge length of a reinforced concrete beam can only be estimated; additional complexity is introduced when relative movement between the constituent components (such as between an unbonded tendon and the surrounding concrete) invalidates the assumption of stress-strain compatibility. The hinge length for the mixed specimens IWS and IWC was estimated two ways: 1) from inspection of the final cracking pattern; and 2) from rigid body mechanics and measured strain and displacements. It is acknowledged that the length of the cracked portion of the beam is not the same as the plastic hinge length; instead, because the cracked length of the beam should be greater than the plastic hinge length, it is used for quick assessment of the $2Z_s$ assumption.

Estimation via final cracking—A qualitative estimate of each specimen's hinge length is estimated through inspection of the final cracking pattern (Fig. 5) and is given

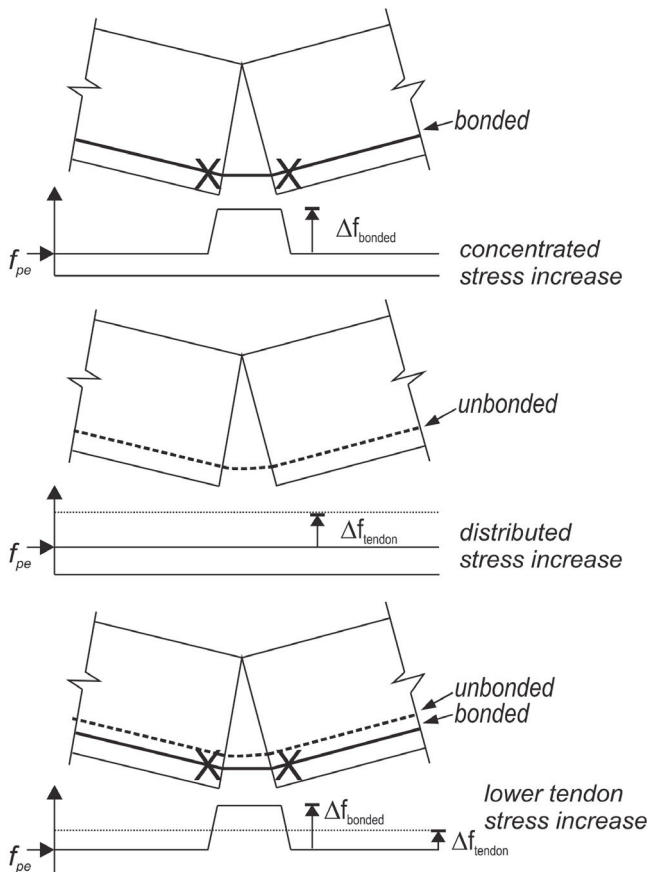


Fig. 10—Tendon force increase: bonded versus unbonded.

Table 6—Hinge length by measured strain and deflection versus $2Z_s$

Specimen	Measured concrete strain, in. ⁻⁶ /in.	Steel strain, in./in.	Measured deflection, in.	Calculated curvature, rad* 10 ⁻⁶ /in.	Cracked length, in.	Hinge length by Eq. (10), in.	$2Z_s$, in.	Hinge length by Eq. (10)/ ($2Z_s$)
IWS	4200	0.06	2.9	1088	47	50	108	0.5
IWC	2600	0.06	5.5	1060	95	69	108	0.6

Note: 1 in. = 25.4 mm.

in Table 6; hinge length is defined by the portion of bottom flange containing visible flexural cracks.

Specimen IGS exhibited well-distributed flexural cracking, as is typical of bonded prestressed beams; with further load application, the steel at each crack location was exposed to a concentrated strain increase. As the load on IGS continued to increase, cracking spread along the length of the beam as the tensile strength of the concrete was overcome at multiple locations and new crack formation occurred until a stable cracked state of the specimen was reached. Additional vertical displacement continued and, at peak load, the deck crushed as Specimen IGS exhibited ductile failure with the strand yielding prior to deck crushing. The spread distribution of cracks reduced the strain concentration at any one crack, leading to a failure governed by the deck concrete’s compressive strength rather than by rupture of the bonded pretensioned strand.

In the loading of IWS and IWC, however, the opening of a primary crack under the load points—and exposure of the unbonded tendon—reduced the development of additional flexural cracking, concentrating the strain of the bonded reinforcement to the primary crack location, which ultimately led to strand rupture at flexural strength. Both Specimens IWS and IWC experienced strand rupture of the bottom pretensioning strand at the primary crack location. The relatively limited crack distribution is attributed to the low levels of bonded reinforcement; a higher ratio of bonded steel is anticipated to result in better crack distribution.

The hinge length estimated via cracking of Specimens IWS and IWC was 47 and 95 in., respectively, and was much less than the cracked portion observed in grouted Specimen IGS (estimated as 248 in.). Inferring that the hinge length is less than the cracked length, neither mixed tendon specimen exhibited a plastic hinge length of the AASHTO-LRFD assumed $2Z_s$, or 108 in. Instead, the cracking indicates an affected compressive zone defined at an angle much less than 45 degrees from the load-point. The affected region was estimated by extending a straight line from the load point to the initiation tips of the outermost cracks visually observed. In Specimen IWS, the final cracking pattern indicates an affected region, or cracked

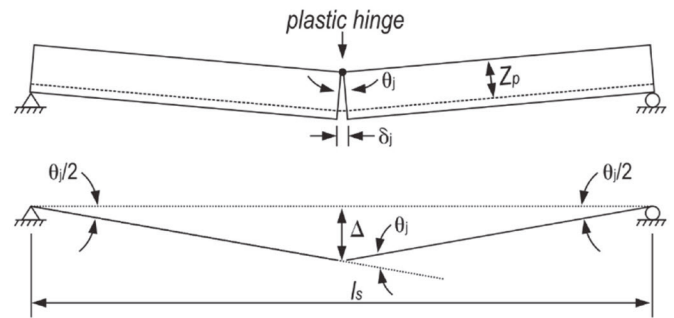


Fig. 11—Rigid body hinge mechanism and geometry of joint opening.

length, defined from approximately 22 degrees from the point load. Specimen IWC had a longer cracked length, as would be expected with the constant moment region. The resulting compressive zone is estimated to affect an area from approximately 17 degrees from the load points.

Estimation via measured strain—Lacking stress-strain compatibility, unbonded tendon stress is dependent on global deformation behavior; MacGregor et al. (1989) described the deformation of unbonded members through the assumption of rigid body motion as the member develops a plastic hinge when approaching flexural strength. The assumed hinge length—or the length of the beam to undergo plasticization—is thereby key to the estimation of the unbonded tendon stress. Although not explicitly described in AASHTO-LRFD (2016), the unbonded tendon stress calculations have been derived considering the hinge length to be $2Z_s$ (refer to MacGregor et al. [1989] and Roberts-Wollman [2005] for the basis of the equations).

The hinge length can be described as a function of measured curvature and deflection.

From rigid body geometry (Fig. 11)

$$\delta_h = \frac{4\Delta Z_p}{l_s} \quad (6)$$

where δ_h is the tendon elongation occurring at the hinge; Δ is the deflection at the hinge; Z_p is the distance between the resultant compressive force and the prestressing

tendon; and l_s is the span length. Assuming the rotation is centered about the resultant compressive force and the curvature at the hinge is constant, the tendon elongation at the hinge

$$\delta_h = \int_0^{l_{hinge}} \Phi_m Z_p(x) \left(\frac{x}{Z_s} \right) dx \quad (7)$$

where l_{hinge} is the length of the hinge; Φ_m is the maximum curvature; and Z_s is the distance from the resultant compressive force to the center of the “passive” steel reinforcement. In previous considerations of unbonded tendons with bonded steel, this was assumed to be bonded mild steel; here it is assumed to be bonded pretensioned steel. Assuming Z_p to be constant over the (assumed small) hinge length

$$\delta_h = \Phi_m \frac{Z_p}{Z_s} \int_0^{l_{hinge}} x dx \quad (8)$$

Solving the integral

$$\delta_h = \frac{\Phi_m Z_p}{2Z_s} l_{hinge}^2 \quad (9)$$

Combining and simplifying Eq. (6) and (10), the hinge length can be described as a function of the maximum curvature and deflection

$$l_{hinge} = \sqrt{\frac{8\Delta Z_s}{l_s \Phi_m}} \quad (10)$$

Based on the measured deck strain and measured tendon force during the ultimate load test, the maximum curvatures for mixed tendon test specimens nearest the failure location were determined using Eq. (10) and are given in Table 6; this is an estimate that assumes the strain gauge, positioned near the load point, was at the location of maximum concrete strain. The steel strain is determined as the rupture strain minus the prestrain (due to prestressing, considering losses); the rupture strain is assumed based on the observed failure mode of the test specimens. The hinge length at flexural strength is calculated by Eq. (10) using measured deflection. Z_s is approximated as the depth to the pretensioned steel, or 59 in.; the tendon length, l_s ,

is 508 in. This estimation of hinge length is compared to that assumed for purely unbonded conditions ($2Z_s$), used in the AASHTO-LRFD (2016) calculation of unbonded tendon stress. For both Specimens IWS and IWC, the hinge length as determined using Eq. (10) is less than $2Z_s$.

Based on the test observations of the cracked beam length, the estimated hinge length via Eq. (10), and the observed flexural strength, flexural strength calculations for members with mixed tendons should be based on a shorter hinge length, especially for members with low quantities of bonded prestressing steel. Assumption of a shorter hinge length would correspond to a lower nominal flexural strength. Additional work to evaluate such conditions, either analytical or experimental, would contribute to the understanding of hinge behavior of mixed tendon systems; the conducted experimental work described herein provides limited insight due to the small number of test specimens.

Tendon stress at flexural strength—The simplified approach given in Section 5.7.3.1.3 of AASHTO-LRFD (2016) for calculation of tendon stress and flexural strength for members with both bonded and unbonded tendons was found to be inaccurate for one of the investigated test specimens. The following discussion compares the observed (measured) tendon stress to that calculated per AASHTO-LRFD (2016) via the simplified approach for components with both bonded and unbonded tendons, which introduces a weighting scheme to account for the presence of both bonded and unbonded tendons.

The AASHTO-LRFD (2016) simplified method for members with mixed tendons allows for an estimation of tendon stress (and all steel stress) via the following approach: 1) the stress in the unbonded tendon is first estimated as the effective prestress after losses f_{pe} ; 2) the stress in the bonded prestressing is then determined by replacing the term $A_{ps} f_{pu}$ in Eq. (5.7.3.1.1-3) and (5.7.3.1.1-4) with $A_{psb} f_{pu} + A_{psu} f_{pe}$; and 3) a weighted (per relative area) average of the bonded and unbonded stress solutions is considered to act over the total area of prestressing steel. It is important to note that the unbonded tendon stress at flexural strength is dependent on the effective prestress. A reasonable estimation of effective prestress is required to ensure an accurate calculation of nominal flexural strength. The weighted unbonded tendon stress for each internal tendon specimen calculated per this approach is given in Table 7 considering test-day material properties.

Hollow-core load cells were used to directly measure the tendon force in the unbonded tendon during the load test. Figure 12 shows the tendon stress versus the applied

moment for the unbonded internal tendon specimens IWS and IWC; the hollow-core load cell on Specimen IGS did not measure a change in tendon stress during the load test and is not shown. Also shown is the actual yield and rupture strength of the prestressing strand per the material certifications. Assuming the full tendon length carries the strain increase caused by the reduced moment of inertia at a crack, Specimens IWS and IWC experience a tendon stress increase at cracking. Crack width measurements were made using crack microscope during load holds at 200 and 250 kip (890 and 1100 kN); these measurements were used to estimate the increase in tendon stress and are shown on the plot. The stress increase estimated using crack measurements appears to correlate to that measured by the hollow-core load cell.

In general, unbonded beams typically reach their maximum load before the tendon stress reaches yield strength. This behavior was observed in Specimen IWS, which achieved maximum load when bonded strands ruptured, prior to the tendon reaching yield. In contrast with the expected behavior, and with Specimen IWS, the tendon in Specimen IWC did surpass the estimated steel yield stress.

In both Specimens IWS and IWC, the tendons exhibited similar behavior. Until each specimen cracked, the measured tendon stress remained nearly at the effective tendon stress. At approximately an applied moment of 2515 kip-ft (37 MN/m)—corresponding to cracking of the specimen—the tendons began to experience increasing tensile stress as the effective prestress was overcome. In both cases, the tendons experienced a similar rate of tendon stress increase. Reflecting the lack of strain compatibility between the concrete and the unbonded tendon, the change in tendon strain due to the applied loads is averaged over the entire tendon length. At pre-cracking loads, the change in tendon strain is low; at post-cracking, significantly larger strain occurs at the crack location and is transferred to the tendon.

In contrast with the expected behavior, and with Specimen IWS, the tendon in Specimen IWC did surpass yield. It is assumed that relatively higher tendon stress in Specimen IWC (versus IWS) is due to the improved distribution of cracks under the constant moment region. Based on the actual stress at 1% elongation reported in the manufacturer supplied material certifications, the tendon had an expected yield at approximately 252 ksi (1740 MPa); the maximum measured tendon stress (via hollow-core load

Table 7—Unbonded tendon stress

Specimen	Weighted per AASHTO-LRFD simplified approach, ksi	Measured, ksi	Measured/weighted
IWS	257	229	0.89
IWC	263	274	1.04

Note: 1 ksi = 6.9 MPa.

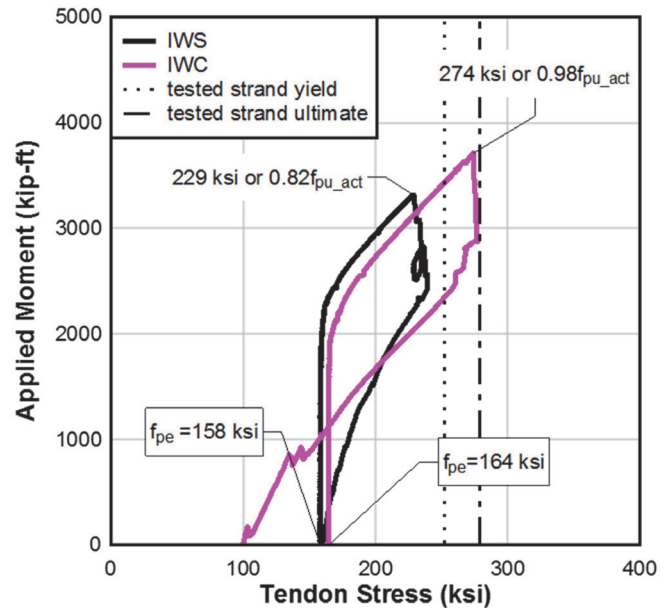


Fig. 12—Applied moment versus measured tendon stress. (Note: 1 in. = 25.4 mm; 1 ksi = 6.9 MPa.)

cell) was approximately 274 ksi (1890 MPa) (Fig. 12). The tendon’s yield is also evident based on the reduced tendon stress remaining in the specimen after unload (100 ksi [690 MPa]) versus the effective tendon stress at the start of the test (164 ksi [1130 MPa]).

SUMMARY AND CONCLUSIONS

Changing the post-tensioning filler material from cementitious grout to flexible fillers (such as wax or grease) in internally post-tensioned girders results in a condition of mixed tendons—a novel reinforcement condition to bridge construction—which affects the overall structural behavior of the system. The use of flexible fillers in post-tensioned bridge construction is new to the United States, and is being investigated by several state departments of transportation for the materials’ potential as a possible component of the corrosion protection system to improve structural system durability and to simplify tendon inspection, maintenance, or replacement.

Experimental and analytical assessment conducted herein to assess members with mixed tendons suggests

this change in filler material may result, when members are lightly reinforced with bonded pretensioned steel in comparatively lower ductility and flexural strength when compared to fully bonded members. This can be accounted for in design through detailed analysis, considering the strain compatibility between the section and the bonded pretensioned steel, when mixed tendon behavior and long-term structural implications are fully understood.

Conclusions

- The hinge length in specimens with mixed tendons (inferred as less than the length of the final cracking patterns) was found to be less than that assumed in the formulation of the unbonded tendon stress equation given in AASHTO-LRFD. Overestimation of the plastic hinge length may lead to a lower estimate of the unbonded tendon stress in calculations of the nominal flexural strength.
 - As in a fully unbonded case, the ductility and strength of members with mixed tendons (members containing
- both bonded and unbonded tendons) are governed by the rotational capacity of the hinge region.
 - The observed flexural strength in the mixed tendon specimens (IWS and IWC) was controlled by bonded strand rupture. This phenomenon limited the stress increase in the unbonded tendons.
 - For single-point loading, concentrated loads in mixed tendon members lightly reinforced with bonded steel, the observed cracked length was approximately d , the depth of the section, and did not correlate well to the AASHTO-LRFD assumed hinge length for unbonded tendons; it is likely that the hinge length will vary in relation to the ratio of bonded and unbonded tendons.
 - The simplified approach given in AASHTO-LRFD (2016) was insufficient to predict flexural strength of the test specimens with mixed bonded and unbonded tendons. Particular care should be taken with low quantities of bonded reinforcement.
- As it stands, little design guidance exists that attempts to address members with mixed bonded and unbonded

Purchase Publications and Register for Events on the PTI Store

The PTI Store makes it easy to find the events (convention, certification workshop, or certification renewal registration) and publications that interest you most. In addition, when purchasing a publication, you will have the ability to select the quantity, format (print or digital), and purchase additional licenses for digital publications—all with a simple drop-down menu.



<http://www.post-tensioning.org/store>



POST-TENSIONING INSTITUTE
Stressing the Stronger Concrete Solution™

components. For one tested specimen, the experimentally observed flexural strength and unbonded tendon stress were less than the values calculated per the current AASHTO-LRFD provisions, suggesting that the simplified approach could potentially lead to unconservative calculations of nominal flexural strength and unbonded tendon stress. It is emphasized, however, that this experimental work evaluated a small quantity of test specimens and further testing should be conducted. Members with mixed bonded and unbonded tendons were found to exhibit behavior different than fully bonded and fully unbonded systems. Further investigation of the parameters influencing the ultimate strength of members with mixed tendons is warranted, as is more expansive design guidance within the structural design specifications.

ACKNOWLEDGMENTS

The authors would like to thank the entire team at the FDOT Marcus H. Ansley Structures Research Lab for their involvement and support. Many thanks to Dura-Stress; Schwager Davis, Inc.; and Civetea for contributing to the test specimen construction. The opinions, findings, and conclusions expressed in this publication are those of the authors and not necessarily those of the Florida Department of Transportation or the U.S. Department of Transportation.

NOTATION

A_{ps} = area of prestressing steel, in.²
 A_{psb} = area of bonded prestressing steel, in.²
 A_{psu} = area of unbonded prestressing steel, in.²
 A_s = area of mild tensile steel, in.²
 A'_s = area of mild compressive steel, in.²
 d_p = distance from extreme compression fiber to centroid of prestressing steel, in.
 d_{pb} = distance from extreme compression fiber to centroid of bonded pretensioned steel, in.
 d_{pu} = distance from extreme compression fiber to centroid of unbonded post-tensioned steel, in.
 f'_c = specified compressive strength of concrete at 28 days, ksi
 f_{pe} = effective stress in prestressing steel at section under consideration after all losses, ksi
 f_{pu} = specified tensile strength of prestressing steel, ksi
 $f_{pu,act}$ = actual test-day tensile strength of prestressing steel, per material certifications, ksi
 f_{ps} = stress in post-tensioning tendon at observed flexural strength, ksi
 f_s = stress in mild steel tension reinforcement at nominal flexural resistance, ksi

f'_s = stress in mild steel compression reinforcement at nominal flexural resistance, ksi

l_{hinge} = length of hinge region, in.

l_s = tendon length, in.

$M_{n,calc}$ = ultimate flexural strength as calculated per AASHTO-LRFD simplified approach, kip-ft

$M_{n,observed}$ = ultimate flexural strength observed during experimental testing, kip-ft

T_b = tension force in bonded steel, kip

T_u = tension force in unbonded steel, kip

Z_p = distance between resultant compressive force and prestressing tendon, in.

Z_s = distance from resultant compressive force to center of bonded pretensioned steel, in.

β_1 = ratio of depth of equivalent uniformly stressed compression zone assumed in strength limit state to depth of actual compression zone

Δ = deflection at hinge, in.

δ_h = tendon elongation occurring at hinge, in.

Φ_m = maximum curvature at strength limit state

REFERENCES

AASHTO, 2016, *AASHTO-LRFD Bridge Design Specifications*, sixth edition with 2016 interim revisions, American Association of State Highway and Transportation Officials, Washington, DC.

Brenkus, N. R.; Wagner, D. J.; and Hamilton, H. R., 2016, "Experimental Evaluation of Flexural Static and Fatigue Strength of an Innovative Splice for Prestressed Precast Concrete Girders," *Journal of Bridge Engineering*, ASCE, V. 21, No. 6, June.

Gauvreau, D. P., 1992, "Load Tests of Concrete Girders Prestressed with Unbonded Tendons," *Report No. 194*, Institute of Structural Engineering ETH Zurich, Birkh ser Publishers, 239 pp.

Gerber, L. L., and Burns, N. H., 1971, "Ultimate Strength Tests of Post-Tensioned Flat Plates," *Journal of the Prestressed Concrete Institute*, V. 16, 6, Nov.-Dec., pp. 40-58.

Hoang, L. H., and Pasquignon, M., 1985, "Essais de Flexion sur des Poutres en Beton Precontraintes par des Cables Exterieurs," *Contrat SETRA CEBTP 1985*, V. 1 and 2, Dossier de Recherche 91017, Nov.

MacGregor, R. J. G.; Kreger, M. E.; and Breen, J. E., 1989, "Strength and Ductility of a Three-Span Externally Post-Tensioned Segmental Box Girder Bridge Model," *Center for Transportation Research Report No. 365-3F*, University of Texas at Austin, Austin, TX, 323 pp.

Mattock, A. H.; Yamazaki, J.; and Kattula, B. T., 1971, "Comparative Study of Prestressed Concrete Beams, With

and Without Bond,” *ACI Journal Proceedings*, V. 68, No. 2, Feb., pp. 116-125.

Megally, S. H.; Garg, M.; Seibel, F.; and Dowell, R. K., 2002, “Seismic Performance of Precast Segmental Bridge Superstructures,” Research Report No. SSRP-2001/24, Structural Systems Research Project, University of California, San Diego, La Jolla, CA.

Ozkul, O.; Nassif, H.; Tanchan, P.; and Harajli, M., 2008, “Rational Approach for Predicting Stress in Beams with Unbonded Tendons,” *ACI Structural Journal*, V. 105, No. 3, May-June, pp. 338-347.

Roberts-Wollmann, C. L.; Kreger, M. E.; Rogowsky, D. M.; and Breen, J. E., 2005, “Stresses in External Tendons at Ultimate,” *ACI Structural Journal*, V. 102, No. 2, Mar.-Apr., pp. 206-213.

Natassia R. Brenkus is an Assistant Professor in the Department of Civil, Environmental, and Geodetic Engineering at The Ohio State University, Columbus, OH. Her research interests include structural concrete behavior, durability, and design.

H.R. Trey Hamilton is Professor of civil engineering at the Engineering School of Sustainable Infrastructure and Environment at the University of Florida, Gainesville, FL. His research and professional interests include structural concrete design and testing, and durability and evaluation of existing bridge and building structures.

Will A. Potter is the Assistant State Structures Design Engineer and Lab Manager at the Marcus H. Ansley Structures Research Center in Tallahassee, FL.

Influence the Future of Post-Tensioning— Join a PTI Technical Committee

All PTI members are encouraged to participate in PTI Technical Committees. Committee participation provides you with the opportunity to learn the latest in post-tensioning technology and play a role in shaping specifications, code development, and publishing industry-standard technical documents.

Committee list and applications available at: www.post-tensioning.org